Vinifa R[1] / Kavitha A[1] / Immanuel Selwynraj A[2]

Power Quality Enhancement Using Lyapunov Based Voltage Source Inverter for the Grid Integrated Renewable Energy System

[1] Department of Electrical and Electronics Engineering, Anna University Chennai, Chennai 600 025, India, E-mail: rvinifa@yahoo.com, akavitha@annauniv.edu. https://orcid.org/0000-0001-7568-5751.
[2] Vellore Institute of Technology, School of Mechanical Engineering, 632 014 Vellore, India, E-mail: aisraj1979@gmail.com

Abstract:
The evolution of high performance power electronic converters makes a feasible way to integrate the Renewable Energy System (RES) to the grid. High performance in terms of stability, good transient and steady state response, load variations is achieved in this work using Current Controlled Voltage Source Inverters (CCVSI) by deriving the control law using Lyapunov function at the expense of a time varying reference current. In this work, a single phase equivalent circuit is represented for the three phase grid connected renewable energy system, and mathematical modeling is developed to design the controller. Analysis using Lyapunov based controller is carried out to ensure the real and reactive power flow from the renewable energy system to the grid connected with the non linear load. The reference current for the controller is generated using the Symmetrical Component theory. This theory requires no transformation and desired source power factor can be achieved. To exhibit the efficacy of the Lyapunov controller, the simulation is carried out using MATLAB/Simulink environment. It is observed that the desired power factor is obtained and Total Harmonic Distortion (THD) is within the IEEE limits in the grid side. The performance of the system is validated experimentally and the results are compared with the conventional hysteresis controller for the same application.

Keywords: current controlled voltage source inverter, symmetrical component theory, Lyapunov function, total harmonic distortion

DOI: 10.1515/ijeeps-2019-0111

Received: May 24, 2019; **Revised:** November 14, 2019; **Accepted:** November 17, 2019

1 Introduction

The extraction of electrical power from renewable energy sources in an efficient way necessitates power electronic interface. But the usage of power electronic equipments produces current harmonics in grid which increases grid current THD and loss in unity power factor [1, 2]. In order to overcome these issues, shunt active power filters are commonly used [3–6]. But this needs an additional circuitry for the power conversion from RES. This can be eliminated by using a current controlled voltage source inverter which serves as a power converter as well as compensator [7–9]. To achieve the above tasks, the generation of reference current is the main part [10]. Usually, based on the characterization of the load and the component to be compensated, the reference current is generated. However, this is not desirable if the load changes frequently [11]. Therefore, it is necessary to use the instantaneous quantities of voltages, currents and power. Some techniques are presented in [12] to generate reference currents using instantaneous values. Among these techniques, instantaneous symmetrical component theory is the only technique that has the capability to change the desired source power factor angle. The non-zero power factor angle reduces the inverter rating compared to zero power factor angle operation [13]. It is simple to implement and requires no transformation [14].

Several current control techniques are proposed in literature [15–20] to follow the reference current for the integration of RES to the grid. The conventional hysteresis controller is simple but it results in variable switching frequency causing more switching losses. Hence the switching frequency can be fixed by comparing with a carrier wave. However in PI controller, the steady state error is present when sinusoidal references are used [13, 14]. The tracking of reference current and the rejection of higher order harmonics in shunt active power filter are better achieved using Repetitive controller [21]. The stability and the transient behavior of shunt active power filter are achieved in [22] along with tracking the reference current. By using shunt active filters, the

Vinifa R is the corresponding author.

control of reactive power is possible. But in this paper, the control of real power flow from RES to grid and load is also achieved using Lyapunov control strategy, which is a vital task for the integration of RES with grid. In addition to the power flow, transient behavior, stability, desired power factor, effect of load variations, and THD reduction are also achieved using Lyapunov control strategy. All the above said tasks are demonstrated in the presence of non linear load. The Lyapunov control strategy is not applied in this scope so far. The Lyapunov control law is derived using the simplified equivalent circuit, thus reducing the complexity in the design. The switching frequency is also fixed by comparing the control input with the carrier signal to generate the pulses reducing the acoustic noise [13].

2 Integration of RES with Grid

Figure 1 shows the general schematic diagram of RESs connected to the utility grid. The power generation from RES varies since it depends on the weather of the region. The maximum power is extracted by the DC/DC converters and AC/DC/AC converter using Maximum Power Point Tracking (MPPT) controller and fed to their corresponding DC and AC loads. These DC and AC microgrids are linked through voltage source inverter. The power flow controller synchronizes the Voltage Source Inverter (VSI) with the grid, mitigates the issues of power quality, controls dc link voltage, real and reactive power.

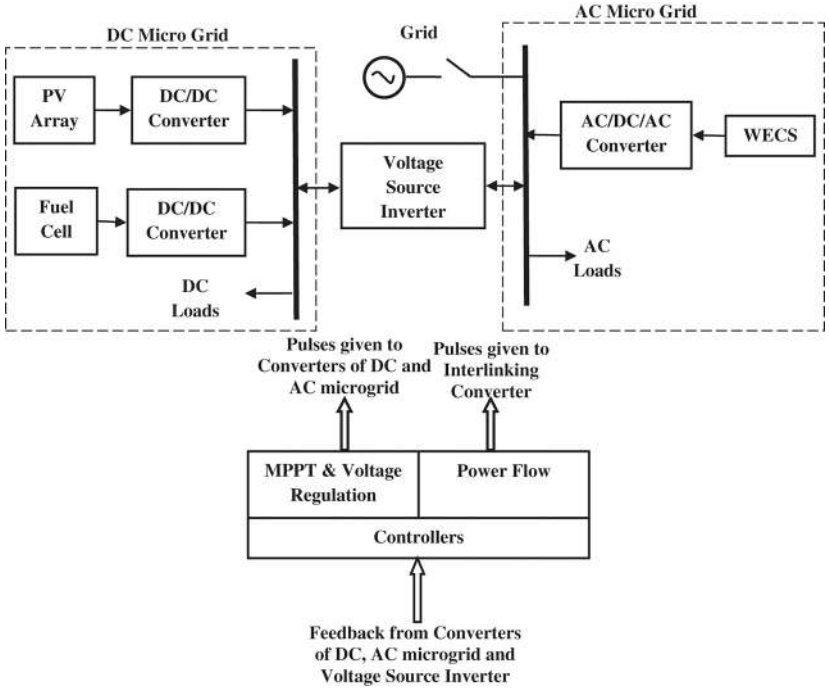

Figure 1: General schematic of RES integrated with grid.

Depending on the power generation from RES (P_c), the extracted maximum power is fed to the loads. If RES power is surplus to supply load, the excess P_{RES} is delivered to the grid. If RES power is lacking to supply load, the deficient load power (P_L) is fed by the grid. But in some poor weather conditions, there will be no power generation in RES. In such circumstances, the entire load power will be met by the grid. But in all the above mentioned cases, the real power is only supplied/absorbed by the grid and the VSI delivers the entire reactive power.

In this work, the control of voltage source inverter is taken into consideration, and hence the RES is assumed as a stiff dc source, V_{dc} as shown in Figure 2. It is connected to the current controlled VSI (CCVSI) which is connected at Point of Common Coupling (PCC) through filter inductances (L_{fa}, L_{fb}, L_{fc}) and R_{fa}, R_{fb}, R_{fc} are the leakage resistances of corresponding filter inductances. A three phase diode bridge rectifier feeding resistive load is used as non linear load, and it is connected at PCC. The non linear load draws harmonic and reactive power components from the grid. The controller is designed to trigger the VSI for maintaining the grid currents sinusoidal by compensating the harmonic components which reduces the THD. The unity power factor operation is also achieved.

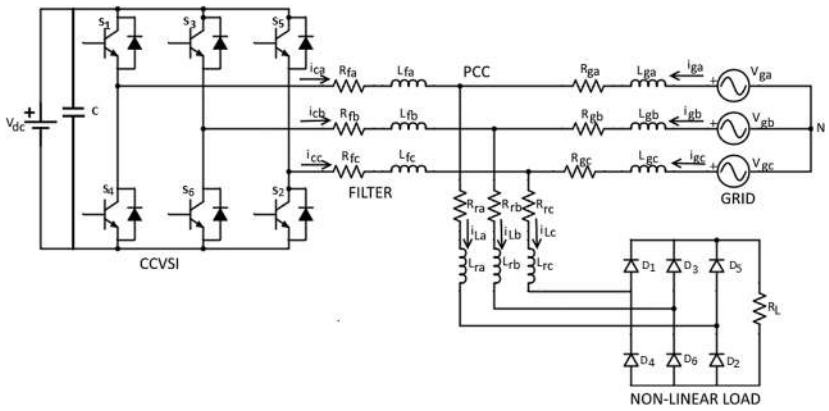

Figure 2: Power circuit diagram of the grid connected inverter.

3 Symmetrical component theory

The symmetrical component theory is based on the instantaneous values rather than average values. This theory is simple and requires no transformation. The prime advantage of this theory is that desired grid power factor can be achieved [14]. The reference currents for the grids (i_{ga}*, i_{gb}*, i_{gc}*) are generated using symmetrical component theory by eq. (1)

$$i^*_{ga} = \frac{v_{ga} + \left(v_{gb} - v_{gc}\right)\beta}{v^2_{ga} + v^2_{gb} + v^2_{gc}}\overline{P_{avg}}$$

$$i^*_{gb} = \frac{v_{gb} + \left(v_{gc} - v_{ga}\right)\beta}{v^2_{ga} + v^2_{gb} + v^2_{gc}}\overline{P_{avg}}$$

$$i^*_{gc} = \frac{v_{gc} + \left(v_{ga} - v_{gb}\right)\beta}{v^2_{ga} + v^2_{gb} + v^2_{gc}}\overline{P_{avg}} \tag{1}$$

Where, $\overline{P_{avg}}$ is the average power supplied by the grid, v_{ga}, v_{gb}, and v_{gc} are the grid voltages for phases 'a', 'b', and 'c', $\beta = \frac{\tan \emptyset}{\sqrt{3}}$, ø is the power factor angle. From the reference grid currents, the inverter reference currents (i_{ca}*, i_{cb}*, i_{cc}*) are found by KCL as in eq. (2)

$$i^*_{ca} = i_{La} - i^*_{ga}$$

$$i^*_{cb} = i_{Lb} - i^*_{gb}$$

$$i^*_{cc} = i_{Lc} - i^*_{gc} \tag{2}$$

Where, i_{La}, i_{Lb} and i_{Lc} are the load currents.

4 Lyapunov based controller

In order to follow the reference current, the pulses are generated for VSI using the Lyapunov based controller. The stability of the system is determined by the Lyapunov Direct method [23]. Along with stability analysis, the Lyapunov controller is used to design the control law using Lyapunov function. To simplify the derivation of control law, the single phase equivalent circuit diagram of grid connected renewable energy system shown in Figure 3 is used to implement the controller.

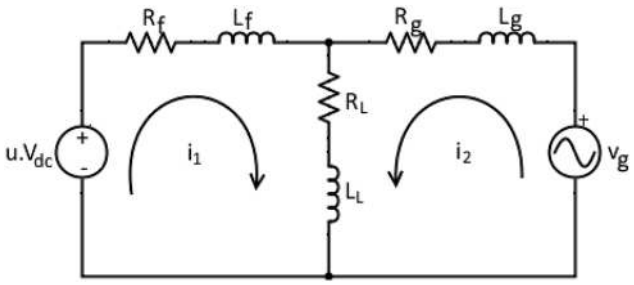

Figure 3: Single phase equivalent circuit diagram.

The mathematical modelling is derived by applying KVL in the single phase equivalent circuit. Now the differential equations are written as

$$R_f i_1 + L_f \frac{di_1}{dt} + R_L (i_1 + i_2) + L_L \frac{d(i_1 + i_2)}{dt} = u.V_{dc}$$

$$R_g i_2 + L_g \frac{di_2}{dt} + R_L (i_1 + i_2) + L_L \frac{d(i_1 + i_2)}{dt} = v_g \tag{3}$$

Taking the loop currents as state variables, the state equations are described as in eq. (4)

$$\begin{pmatrix} \dot{x}_1 \\ \dot{x}_2 \end{pmatrix} = \begin{pmatrix} a_{11} & a_{12} \\ a_{21} & a_{22} \end{pmatrix} \begin{pmatrix} x_1 \\ x_2 \end{pmatrix} + \begin{pmatrix} b_{11} & b_{12} \\ b_{21} & b_{22} \end{pmatrix} \begin{pmatrix} v_g \\ u \end{pmatrix}$$

$$\text{i.e.) } \dot{X} = AX + BU \tag{4}$$

Where $x_1 = i_1$ and $x_2 = i_2$ are the state vectors, v_g is the exogenous input, u is the control input. Other coefficients are represented in eq. (5)

$$\begin{aligned} a_{11} &= \frac{-(R_f+R_L)L_g - R_f L_L}{(L_f+L_L)L_g + L_f L_L} & a_{12} &= \frac{-R_L L_g + R_g L_L}{(L_f+L_L)L_g + L_f L_L} \\ a_{21} &= \frac{-R_L L_f + R_f L_L}{(L_f+L_L)L_g + L_f L_L} & a_{22} &= \frac{-(L_f+L_L)R_g - R_L L_f}{(L_f+L_L)L_g + L_f L_L} \\ b_{11} &= \frac{-L_L}{(L_f+L_L)L_g + L_f L_L} & b_{12} &= \frac{V_{dc}L_g + V_{dc}L_L}{(L_f+L_L)L_g + L_f L_L} \\ b_{21} &= \frac{L_f+L_L}{(L_f+L_L)L_g + L_f L_L} & b_{22} &= \frac{-V_{dc}L_L}{(L_f+L_L)L_g + L_f L_L} \end{aligned} \tag{5}$$

Where, v_g is the grid voltage and u is the switching control variable. From the mathematical model, the control law is derived based on the energy function (V) which cannot increase with time. The positive definite Lyapunov energy function (V) is defined as in eq. (6)

$$V = \frac{1}{2} e^T e \tag{6}$$

Where error is represented as $e = x_1^* - x_1$, x_1^* is the tracking reference of x_1.

Differentiating eq. (6) with respect to time becomes eq. (7)

$$\frac{dV}{dt} = e^T \frac{de}{dt} \tag{7}$$

By making the control input (u) to converge the error (e) as zero, the derivative of Lyapunov function should be negative definite. In the present case, it is chosen as in eq. (8)

$$\frac{dV}{dt} = -e^T \lambda e \tag{8}$$

Where, λ is the strictly positive value. Comparing eqs. (7) and (8), the control input u is derived by applying the Lyapunov function and found as in eq. (9)

$$u = \frac{1}{b_{12}}\left[\frac{dx_1^*}{dt} - a_{11}x_1 - a_{12}x_2 - b_{11}v_g + \lambda_1 e_1\right] \tag{9}$$

The control signal is compared with the carrier signal to generate the pulses with fixed switching frequency. The block diagram of control scheme of inverter using Lyapunov controller is shown in Figure 4.

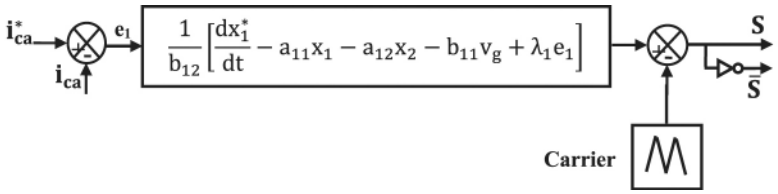

Figure 4: Control diagram of the inverter for phase 'a' using Lyapunov controller.

In order to determine the stability, 'u' in eq. (9) is substituted in eq. (4) and the matrix A is modified as

$$A_{mod} = \begin{pmatrix} 0 & 0 \\ a_{21} + \frac{b_{22}}{b_{12}}a_{11} & a_{22} + \frac{b_{22}}{b_{12}}a_{12} \end{pmatrix} \tag{10}$$

The eigen values are determined as negative real part, hence the system is stable.

5 Simulation results and discussions

The system specifications tabulated in Table 1 is simulated using MATLAB simulink environment. The inverter output voltage V_0 is $mV_{dc}/2$, where m is the modulation index. Here 'm' is taken as 0.67. The Lyapunov based controller controls the CCVSI to reduce the grid THD and improve the power factor under load variations. It also controls real and reactive power flow for different RES power. The sign convention followed for power flow is assumed to be positive when the power flows from grid/inverter to PCC and is negative when the power flows from load to PCC. To visualize the voltage current waveforms clearly, the load current, grid current and inverter current are amplified with a factor of 10, 40 and 10 respectively.

Table 1: Parameters of the simulation circuit.

Parameters	Values
DC Link Voltage	300 V
Grid side Voltage (max. value)	100 V
CCVSI filter Inductance	50 mH
CCVSI filter Resistance	0.4 Ω
Feeder Inductance	0.01 mH
Feeder Resistance	1 Ω
Rectifier Link Inductance	40 μH
Rectifier Link Resistance	0.1 Ω
Rectifier DC side Resistance	50 Ω

5.1 Connection of CCVSI to the grid

The Lyapunov controller for the grid interfacing inverter connected to the non-linear load is analyzed in this section. Figure 5 shows the inverter, grid, load voltages and currents before and after connection of CCVSI to the grid. Initially, the CCVSI is not connected to the system for time, $t < 0.1$ s. During this time, the grid current is same as the load current which contains the harmonic current components of the non linear load. The CCVSI is connected to the system at $t = 0.1$ s, and the CCVSI starts injecting the reactive power requirement of non-linear load so that the grid current is changed from non linear current to sinusoidal current. As it can be seen, the controller takes only 0.2 ms for the grid current to follow the grid voltage. It is also found that the CCVSI

compensates the harmonic and reactive power components making the grid current sinusoidal and unity power factor operation in the grid side.

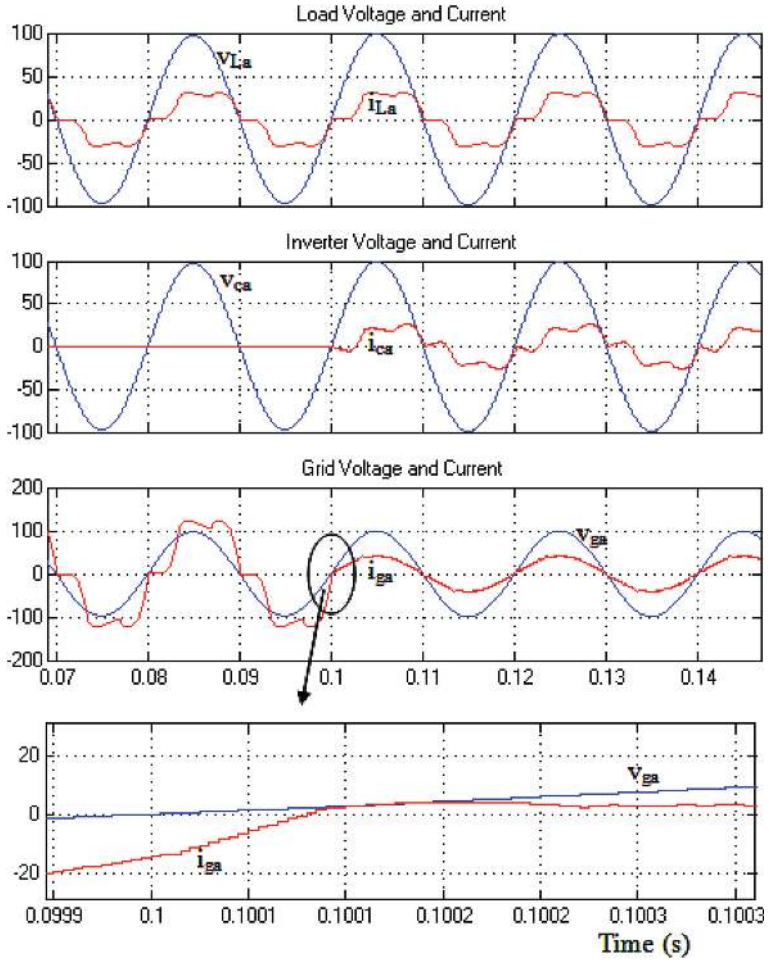

Figure 5: Simulated waveforms of load, inverter, grid voltages and currents before and after compensation.

5.2 Effect of change in load

To validate the performance of the Lyapunov controller, the load resistance is increased from 50 Ω to 100 Ω at t = 0.1s with constant real power of grid. Figure 6 shows the load, inverter, grid voltages and currents for a change in load resistance. For the load resistance of 50 Ω (t < 0.1s), the rms load, inverter and grid currents are 2.03 A, 1.3 A and 0.73 A respectively and at t = 0.1 s the load resistance is changed to 100 Ω. Now the rms load and inverter currents are reduced to 1.23 A and 0.5 A, but there is no change in grid current due to constant real power of grid. It is inferred from Figure 6, the grid current is not affected due to the load change and is free of harmonics achieving unity power factor operation in both the load resistances.

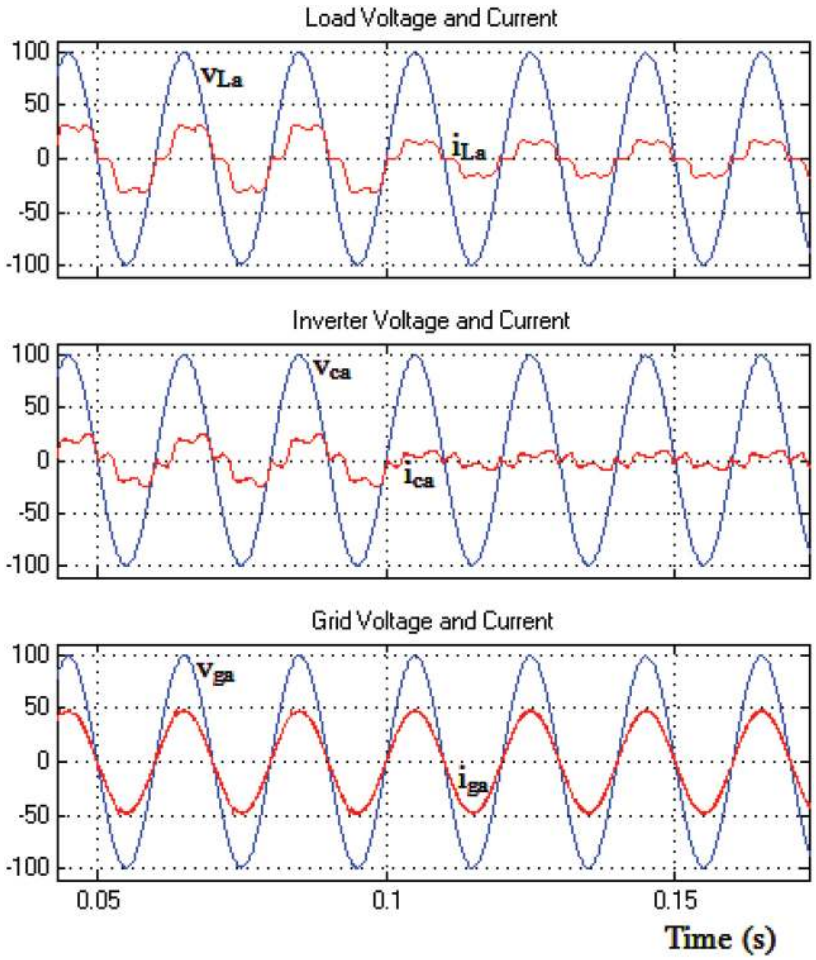

Figure 6: Simulated results of load, inverter, grid voltages and currents under changes in load from 100 Ω to 50 Ω.

5.3 Real and reactive power flow for different RES powers

The power generation in the RES varies depending upon the climatic conditions. Three different modes of operation depending on the source power are considered as shown in Figure 7. The mode 1 is grid supplying the entire real power and no RES power but CCVSI supplies the entire reactive power. The other modes are the RES power is lesser and greater than load power.

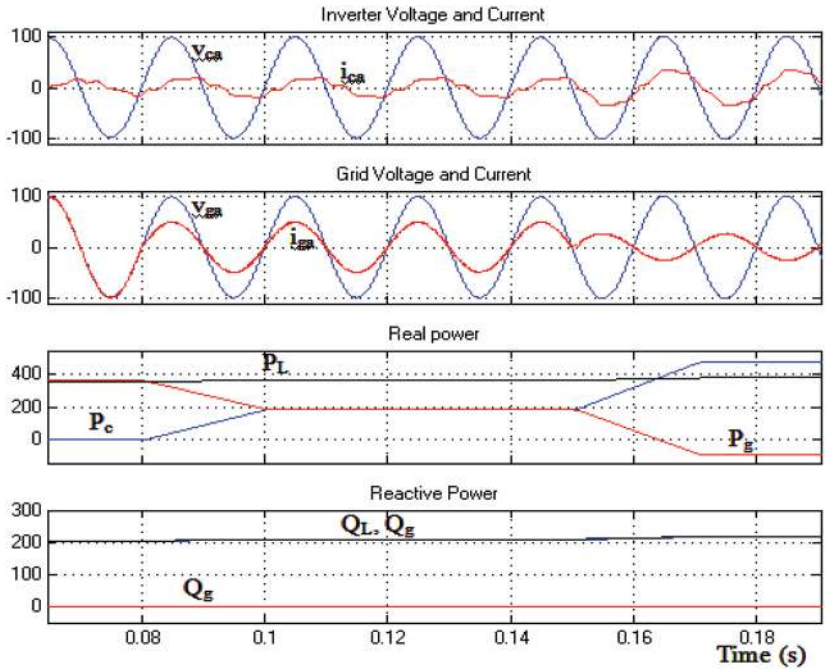

Figure 7: Simulated results of load, inverter, grid voltages, currents, real and reactive power under three modes of operation.

5.3.1 Mode 1 (0 < t < 0.08 s)

In this case, the power generation in RES is assumed to be zero. During this time, the VSI supplies the entire reactive power (Q_c), and the whole of real power required by the load (P_L) is supplied by the grid (P_g). Therefore the grid voltage and current are in phase with each other.

5.3.2 Mode 2 (0.08 s < t < 0.15 s)

In this case, the power generation from RES is considered lesser than the load power (P_L). The load real power is shared by the grid and the VSI. The entire reactive power is supplied by the VSI. Hence the grid voltage and current are in phase with each other.

5.3.3 Mode 3 (t > 0.15 s)

Here, the RES power is taken greater than the load power (P_L). The excess RES power is supplied to the grid; hence the grid voltage and current are out of phase with each other. The reactive power is supplied by the VSI.

Due to fast dynamics of Lyapunov controller, both the inverter and grid current exhibit good transient response for changes in real power as shown in Figure 7.

5.4 Achievement of desired power factor

The desired power factor can be achieved by varying the power factor angle (ø). Figure 8 shows the grid voltage and current for angles 5° and 10°. If power factor is varied to 0.99 or 0.98 rather than unity power factor, the VSI rating will be reduced which makes the system economical.

5.5 Power factor and THD analysis

The reactive power components present in the load affects the grid which makes the power factor to 0.862 before the VSI is connected to the grid. The non-sinusoidal current drawn by the load produces harmonics with THD of

12 % in the grid. Later, when the CCVSI is connected, it improves the power factor by compensating the reactive power components and is shown in Table 2. From the table, it is inferred that the THD is reduced to 1 % and power factor to 0.999 is achieved. The performance of the Lyapunov controller is validated by maintaining the THDs within the IEEE limits (<5 %) in all the scenarios.

Table 2: Power factor and THD values at phase 'a'.

Scenario	Conditions	Power factor	THD (%)
Connection of CCVSI to grid	Before Connection	0.862	12
	After Connection	0.999	1
Change in load resistance	100 Ω	0.999	1
	50 Ω	0.999	1
Sharing of real and reactive power	Mode 1	1	0.5
	Mode 2	0.9999	1
	Mode 3	−0.9997	2
Change in power factor angle	5°	0.9963	1
	10°	0.9853	0.98

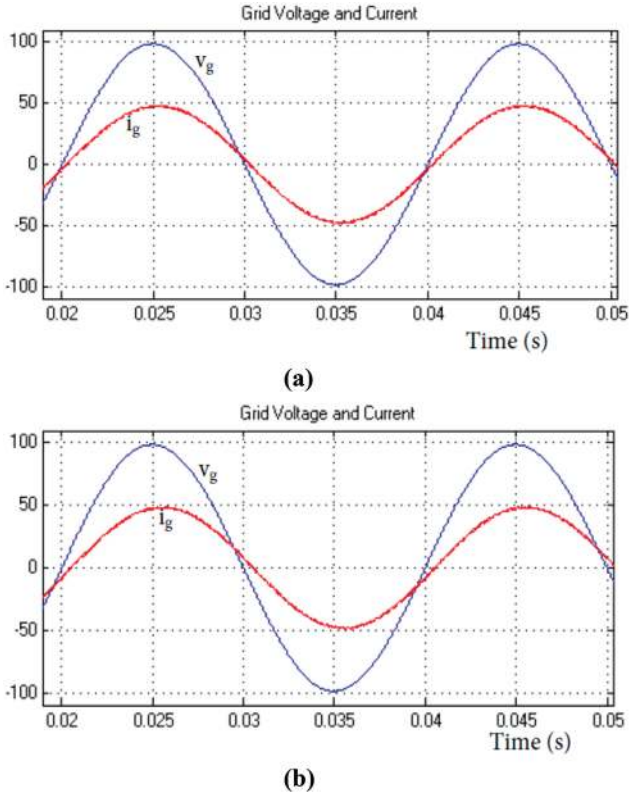

Figure 8: Simulated results of grid voltage and current in phase 'a' for different power factor angles (a) ø = 5° and (b) ø = 10°.

6 Experimental results and discussions

The experimental prototype shown in Figure 9 has been developed for the same specifications specified in Table 1. The prototype consists of inverter unit, filter unit, grid section, load, sensors and control unit. The inverter unit is made up of intelligent power modules with voltage 600 V. It comprises of single phase rectifier feeding input to the inverter and built-in driver circuit to amplify the pulses generated by the controller. An inductor is used as filter which is connected to the grid using autotransformer. A diode bridge rectifier (TSPR60PB) feeding resistance is connected at the point of common coupling. The voltages and currents are sensed by voltage sensors (LV25-P) with voltage range of 10–500 V and current of 10 mA and current sensors (LTS25-NP) with current range of 25 At respectively. The reference current generation and Lyapunov control are implemented in FPGA Spartan 6. The experimental waveforms of inverter, grid, load voltages and currents for mode 1, mode

2 and mode 3 operations using hysteresis and Lyapunov controller are shown in Figure 10 and Figure 11 respectively. The load absorbs 150 W of real power. In mode 1 and mode 2, the grid current flows towards PCC since the grid feeds the load entirely and partially respectively. Therefore, the grid voltage and current are in phase with each other. But in mode 3, the direction of grid current changes since the surplus power in RES feeds the grid in addition to the load. Therefore, the grid voltage and current are out of phase with each other. The THDs obtained in the grid current for modes 1, 2 and 3 are 5.6 %, 6 % and 6.9 % using hysteresis controller, 2.7 %, 4 % and 3.8 % using Lyapunov controller. The power factor in the grid side is 0.98, 0.96 and −0.93 using hysteresis controller and 0.993, 0.984 and −0.994 using Lyapunov controller for modes 1, 2 and 3 respectively. The comparison between hysteresis and Lyapunov controller is shown in Figure 12. It is inferred that the THD and power factor is better using Lyapunov controller compared to the hysteresis controller.

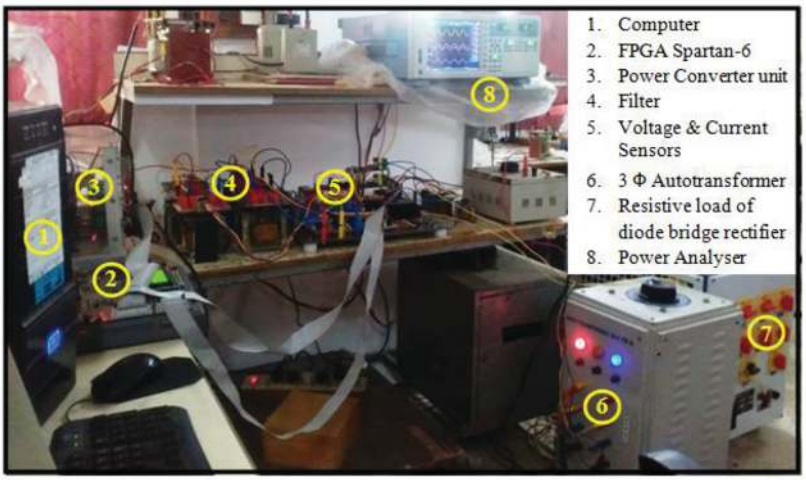

Figure 9: Experimental setup.

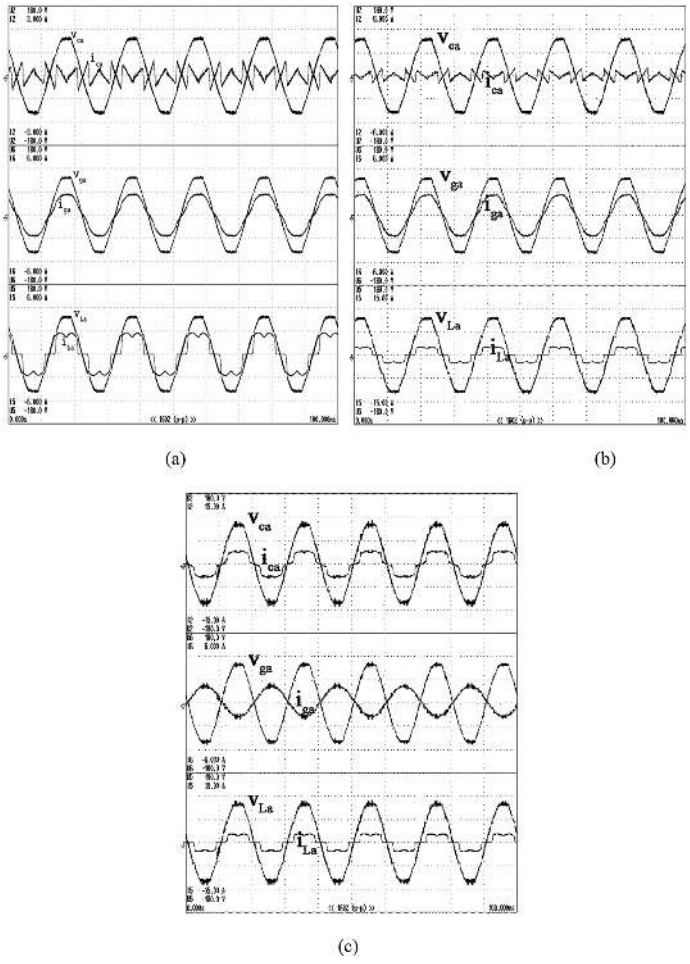

Figure 10: Experimental results of hysteresis controller (a) Mode1 operation, (b) Mode 2 operation, (c) Mode 3 operation.

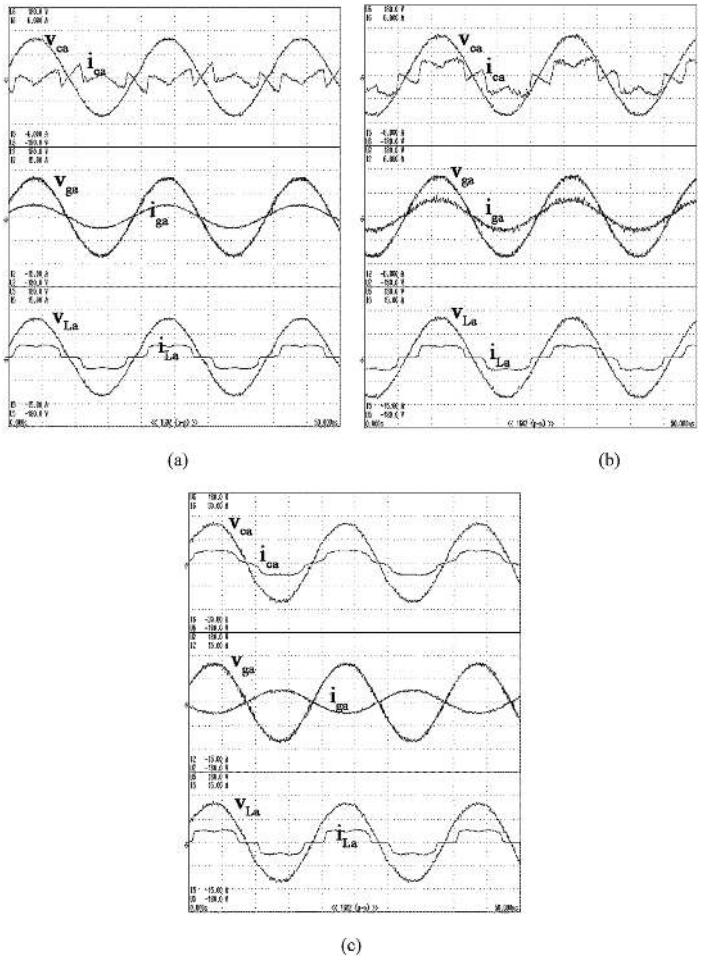

Figure 11: Experimental results of Lyapunov controller (a) Mode1 operation, (b) Mode 2 operation, (c) Mode 3 operation.

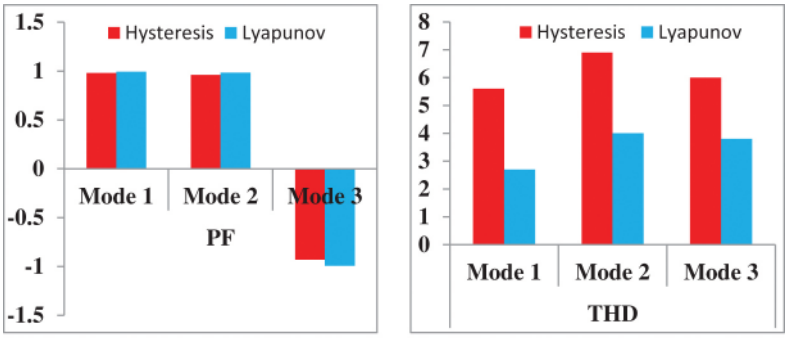

Figure 12: Comparison of measured values between hysteresis and Lyapunov controller (a) Power factor (b) THD.

Figure 13 shows the experimental results for a different load of 140 W under mode 2 operation. From the fig., it is observed that the grid current is sinusoidal with free of harmonics and power factor is nearer to unity even under the different load.

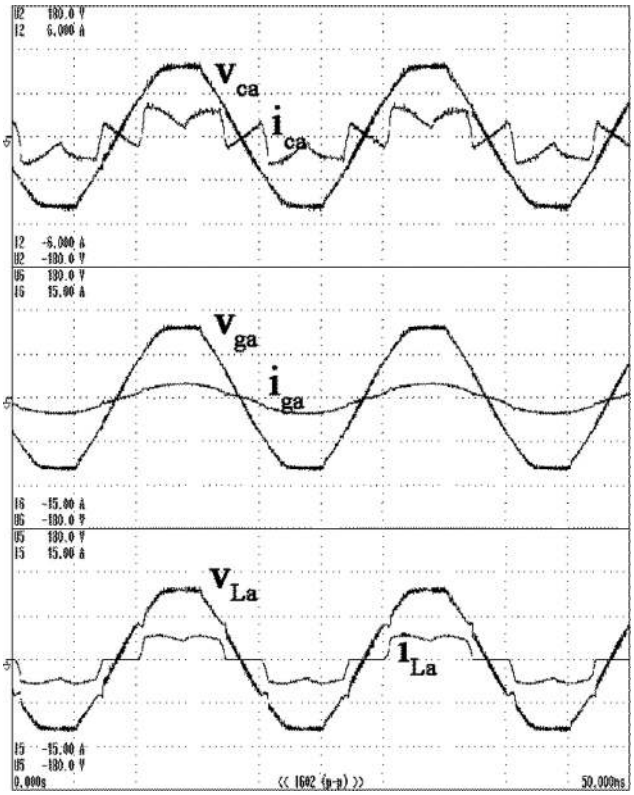

Figure 13: Experimental results for a load of 140 W in mode 2 operation.

7 Conclusion

A Lyapunov control strategy for the grid integration of renewable energy system is presented. The control law is derived using the simplified equivalent circuit, and it reduces the complexity. The CCVSI compensates the harmonic current and reactive power components drawn by the non linear load attaining harmonic free current and unity power factor in the grid side. The performance of the Lyapunov controller is satisfactory in both transient and steady state response. The real and reactive power flow from RES to the grid is varied in 3 modes for different power generation in RES conditions. It provides outstanding results in all the 3 modes by giving low THD and unity power factor. The desired power factor is obtained by using the symmetrical component theory which is implemented in a-b-c frame. The validity of Lyapunov controller performance results is compared with hysteresis controller.

References

[1] Schavemaker P, Sluis PV. Electric power system essentials. West Sussex, England: John Wiley and Sons Ltd.; 2008. p. 221–36.
[2] Meral E, Çelik D. Grid tied fuel cell system using single phase PLL based SOGI with PI and PR current controllers. Universal J Electr Electron Eng. 2016;4:91–6.
[3] Garica-Gonzalez P, Garcia-Cerrada A. Control system for a PWM-based STATCOM. IEEE Trans Power Delivery. 2000;15:1252–7.
[4] Rao P, Crow ML, Yang Z. STATCOM control for power system voltage control applications. IEEE Trans Power Delivery. 2000;15:1311–17.
[5] Norouzi AH, Sharaf AM. Two control schemes to enhance the dynamic performance of the STATCOM and SSSC. IEEE Trans Power Delivery. 2005;20:435–42.
[6] Hooshmand RA, Esfahani MT. A new combined method in active filter design for power quality improvement in power systems. ISA Trans. 2011;50:150–8.
[7] Vinifa R, Kavitha A. Enhancement of power quality using double band hysteresis controller for the grid integrated renewable energy system. Int Trans Electr Energy Syst. 2018;28:1–17.
[8] Vinifa R, Kavitha A, Immanuel SA. Power quality enhancement using linear quadratic regulator based current-controlled voltage source inverter for the grid integrated renewable energy system. Electric Power Comp Sys. 2017;45:1783–94.
[9] Vinifa R, Kavitha A. Linear quadratic regulator based current control of grid connected inverter for renewable energy applications. In: IEEE Conf on Energy Efficient Technologies for Sustainability (ICEETS), Nagercoil, India, 2016.

[10] Meral E, Celik D. Comparison of SRF/PI-and STRF/PR-based power controllers for grid-tied distributed generation systems. Electr Eng. 2018;100:633–43.
[11] Ghosh A, Ledwich G. Power quality enhancement using custom power devices, 1st ed. New York: Springer Publishers, 2002:241–86.
[12] Agaki H, Wantanabe EH, Aredes M. Instantaneous power theory and applications to power conditioning. IEEE Press, NJ: John Wiley and Sons Ltd., 2007:19–40.
[13] Rajendran S, Govindarajan U, Reuben AB, Srinivasan A. Shunt reactive VAR compensator for grid-connected induction generator in wind energy conversion systems. IET Power Electron. 2013;6:1872–83.
[14] Ghosh A, New A. Approach to load balancing and power factor correction in power distribution system. IEEE Trans Power Delivery. 2000;15:417–22.
[15] Celik D, Meral ME. A novel control strategy for grid connected distributed generation system to maximize power delivery capability. Energy. 2019;186:115850.
[16] Timbus A, Liserre M, Teodorescu R, Rodriguez P, Blaabjerg F. Evalution of current controllers for distributed power generation system. IEEE Trans Power Electron. 2009;24:654–63.
[17] Hornik T, Zhong QC. A current-control strategy for voltage-source inverters in microgrids based on $H\infty$ and repetitive control. IEEE Trans Power Electron. 2011;26:943–52.
[18] Chen Y, Smedley K. Three-phase boost-type grid-connected inverter. IEEE Trans Power Electron. 2008;23:2301–9.
[19] Celik D, Meral ME. Current control based power management strategy for distributed power generation system. Control Eng Pract. 2019;82:72–85.
[20] Kawasaki N, Nomura H, Masuhiro M. A new control law of bilinear dc-dc converters developed by direct application of Lyapunov. IEEE Trans Power Electron. 1995;10:318–25.
[21] Costa-Castello R, Grino R. Odd-harmonic digital repetitive control of a single-phase current active filter. IEEE Trans Power Electron. 2004;19:1060–8.
[22] Komurcugil H, Kukrer O. A new control strategy for single-phase shunt active power filters using a Lyapunov function. IEEE Trans Ind Electron. 2006;53:305–12.
[23] Bogdan MW, Irwin JD. Control and mechatronics, 2nd ed. Florida, United States: CRC Press, 2011.